Hyperbolic Lattice Boltzmann Method and Discrete Boltzmann Method for Solid-Liquid Phase Change Problem

Snehil Srivastava[1*] and Panchatcharam Mariappan[1]

[1]Department of Mathematics and Statistics, Indian Institute of Technology, Tirupati, 517619, Andhra Pradesh, India.

*Corresponding author(s). E-mail(s): snehilsrivastava59@gmail.com;

Abstract

The Lattice Boltzmann Method (LBM) is a potential numerical tool for solving challenging fluid problems. The Bhatnagar Gross Krook (BGK) approximation is incorporated in the extensively used LBM-BGK approach. In the Hyperbolic Lattice Boltzmann Method (HLBM), a hyperbolic collision operator is used for the collision process, whereas the essential objective of Multiple Relaxation Time (MRT) collision operators is to manage the relaxation of different moments independently to boost accuracy and stability. In this paper, to solve the solid-liquid phase change problem, the HLBM and MRT Discrete Boltzmann Method (DBM) are coupled with the enthalpy method to observe the phase change phenomenon governed by the heat conduction phenomenon.

Keywords: Hyperbolic Lattice Boltzmann, Discrete Boltzmann, Phase Change, Multiple Relaxation Time

1 Introduction

Phase change problem is pervasive in many engineering applications such as alloys solidification, energy storage, and many more. The differential equation can be used to determine the nature of these phase changes, but solving it can be challenging because it contains a non-linear term. As a result, numerical

methods have been developed because analytical solutions are primarily constrained to problems with straightforward geometry and boundary conditions. With the advancement of microscale processing technology in recent decades, solid-liquid phase issues with microscale alteration, including laser cutting [1] and selective laser melting (SLM) [2], have gotten more and more attention. Due to the difficulty in the phase transition process, researchers have suggested several numerical approaches. These methods fell into two categories: one deals with the solid-liquid interface utilizing a fixed grid method and the other deals with a distorted mesh or transformed coordinate system. The distorted mesh has drawbacks of complicated coding and prolonged computation, whereas the fixed grid technique does not have this problem. Voller et al. [3] have discussed the multiple fixed grid methods for phase change problems; however, the enthalpy approach [4] and the equivalent heat capacity method [5] are the most frequently employed fixed grid methods.

Jiaung et al. [6] combined the lattice Boltzmann method with the enthalpy method to solve the phase change problem by processing the phase change term or the source term using the finite difference method, which involves iterative calculation. Huang et al. [7] used the modified equilibrium distribution function to avoid the iteration step in the source term and make it a little bit simpler.

Ahmed [8] developed the idea of a double distribution function combined with an enthalpy method, while Chatterjee [9] introduced a passive scalar-based thermal LBM paired with a fixed grid porosity approach to solving phase change problems.

The discrete Boltzmann technique is a revolutionary LBM variation that only uses one distribution function to determine numerous macroscopic characteristics like temperature, velocity, density, etc. Furthermore, it captures the hydrodynamic and thermodynamic nonequilibrium effects of fluid flow. DBM has advanced significantly during the past few decades. Many researchers have modeled the multiphase flow [10] while considering the gradient and interparticle forces. Zhang et al. [11] suggested a simplified Enskog expansion-based kinetic model for multiphase flow. However, all of these were based on the BGK approximation, i.e., the Single Relaxation Time (SRT) model. On the other hand, in the MRT DBM [12] for compressible exothermic flows, each distribution function is relaxed at a different pace toward the equilibrium position. BGK operator is a specific instance of MRT operator, whereas MRT operator is the general type of collision operator that is more stable and improves the accuracy [13, 14].

The non-Fourier effect is currently excluded by the DBM, which is based on the BGK approximation and MRT operator. Therefore, taking into account the non-Fourier effect demands additional investigation.

To combat this, Cattaneo [15] and Vernotte [16] introduced the CV model, which takes the non-Fourier effect into account to solve the hyperbolic heat equation. Using this model, Liu et al. [17] developed the notion of HLBM. From a mathematical perspective, the HLBM can be used to solve the hyperbolic equation, whereas the LBM can be used to solve the parabolic equation.

This work shows the temperature distribution of Fourier and non-Fourier heat conduction using HLBM and DBM, involving the enthalpy technique and Jiaung's theory [6].

2 Enthalpy Method

The enthalpy approach is typically one of the best methods for modeling solid-liquid phase change problems. The governing equations are stated in terms of overall enthalpy and thus are expressed as:

$$\frac{\partial(\rho H)}{\partial t} = \nabla.(K\nabla T) \tag{1}$$

The density, the thermal conductivity, and the total enthalpy is represented by ρ, K, and H, respectively, where H is expressed in terms of the sensible enthalpy and the latent heat as,

$$H = C_p T + f_l L_a \tag{2}$$

where C_p symbolizes for specific heat at constant pressure, T for temperature, L_a for latent heat of phase change, and f_l for liquid phase fraction. During phase transformations, the value of the phase fraction always fluctuates between zero to one. It carries a value of 1 for liquids and 0 for solids. Using (2) in (1)

$$\frac{\partial(\rho C_p T)}{\partial t} = \nabla.(K\nabla T) - L_a \frac{\partial(\rho f_l)}{\partial t} \tag{3}$$

Here, ρ, C_p and K are constants, therefore, equation (3) can be rewritten as:

$$\frac{\partial T}{\partial t} = \nabla.(\alpha\nabla T) - \frac{L_a}{C_p}\frac{\partial f_l}{\partial t} \tag{4}$$

where, $\alpha = \frac{K}{\rho C_p}$ is the thermal diffusivity.

Equation (4) describes the Fourier heat conduction equation with phase change, although no consideration was made for the non-Fourier effect. The Fourier law assumes that the rate of heat transmission is limitless. However, it is invalidated by many factors, such as high heat fluxes, short intervals, and low temperatures. Cattaneo and Vernotte considered the non-Fourier effect, where the rate of heat transmission is restricted, as a solution to this issue. They have identified the erratic behavior of heat conduction and speculated that relaxation time would play an essential role in this.

3 Hyperbolic Lattice Boltzmann method for heat conduction with phase change

3.1 CV Heat Conduction Problem

The CV heat transfer equation with phase change is given by [18]

$$\frac{\partial T}{\partial t} + \tau \frac{\partial^2 T}{\partial t^2} = \alpha \nabla^2 T + \frac{L_a}{\rho C_p}\left(g + \tau \frac{\partial g}{\partial t}\right) \tag{5}$$

The above equation's LBM form is

$$f_i(x + dx, t + dt) - f_i(x, t) = \Lambda[f_i(x, t) - f_i^{eq}(x, t)] + \frac{L_a w_i \Delta t}{\rho C_p} g_i \tag{6}$$

Here, τ is the relaxation time and when it is zero and $g = -\frac{\partial(\rho f_l)}{\partial t}$, the equation (5) reduces to equation (4). The hyperbolic collision operator Λ for 1D is given by [18]

$$\Lambda = -\frac{2\Delta x^2 \left(1 + \tau \frac{\partial}{\partial t}\right)}{2\alpha \Delta t + \Delta x^2 \left(1 + \tau \frac{\partial}{\partial t}\right)} \tag{7}$$

Substituting the value of Λ in equation (6), we obtain

$$\psi_i = \phi \psi_i^0 - 2(\phi + \varphi)\theta_i + 2\phi \theta_i^0 + \frac{w_i \Delta t}{\rho C_p}(g_i - g_i^0) \tag{8}$$

Here, $\psi_i(x,t) = f_i(x + \Delta x, t + \Delta t) - f_i(x,t)$, $\psi_i^0(x,t) = \psi_i(x, t - \Delta t)$, $\theta_i(x,t) = f_i(x,t) - f_i^{eq}(x,t)$, $\theta_i^0 = \theta_i(x, t - \Delta t)$, $\phi = \frac{\gamma}{2\alpha^* + 1 + \gamma}$, $\varphi = \frac{1}{2\alpha^* + 1 + \gamma}$, $\alpha^* = \frac{\alpha \Delta t}{\Delta x^2}$, $\gamma = \frac{\tau}{\Delta t}$ and $g_i^0(x,t) = g_i(x, t - \Delta t)$

3.1.1 2D CV Heat Conduction Problem

The equation (5) can be rewritten as:

$$\frac{\partial T}{\partial t} = \frac{\alpha}{1 + \tau \frac{\partial}{\partial t}} \nabla^2 T + L_a \frac{g}{\rho C_p} \tag{9}$$

The equation (5) LBM form is

$$f_i(x + c_i \Delta t, t + \Delta t) - f_i(x, t) = \Lambda[f_i(x, t) - f_i^0(x, t)] + \Delta t \Theta_i \tag{10}$$

In this instance, f_i and f_i^{eq} denote the particle distribution function and equilibrium distribution function in the i^{th} direction, respectively. The time step is denoted by Δt, the size of the lattice is denoted by Δx, and the source term,

also known as the phase change term, is denoted by Θ_i which affects the distribution function and comes from the direction i in a lattice, Θ_i is taken as $\Theta_i = w_i L_a \frac{g}{\rho C_p}$, and the collision operator we require is denoted by Λ.

$$f_i^0 = w_i T \tag{11}$$

The weight functions for each distribution function are denoted by w_i. The Taylor series expansion of $f_i(x + c_i\Delta t, t + \Delta t)$ around (x, t) is given as:

$$\begin{aligned} f_i(x + c_i\Delta t, t + \Delta t) = f_i(x,t) + \Delta t\partial_t f_i + \Delta t\partial_{x_\alpha} c_{i_\alpha} f_i \\ + \frac{1}{2}(\Delta t)^2(\partial_t\partial_t f_i + 2\partial_t\partial_{x_\alpha} c_{i_\alpha} f_i + \partial_{x_\alpha}\partial_{x_\beta} f_i) + O(\Delta t^3) \end{aligned} \tag{12}$$

Substituting equation (12) in equation (10) gives:

$$\begin{aligned} \Delta t\partial_t f_i + \Delta t\partial_{x_\alpha} c_{i_\alpha} f_i + \frac{1}{2}(\Delta t)^2(\partial_t\partial_t f_i + 2\partial_t\partial_{x_\alpha} c_{i_\alpha} f_i + \partial_{x_\alpha}\partial_{x_\beta} f_i) \\ = \Lambda[f_i(x,t) - f_i^0(x,t)] + \Delta t\Theta_i \end{aligned} \tag{13}$$

The distribution function has the following constraint:

$$\sum_i f_i^0 = T \tag{14}$$

$$\sum_i f_i^r = 0, (r \geq 1) \tag{15}$$

Introducing the Knudsen number ϵ [14]

$$\partial_t = \epsilon^2\partial_{t^{(2)}}, \partial_{\mathbf{x}} = \epsilon\partial_{\mathbf{x^{(1)}}} \tag{16}$$

where $t^{(2)}$ represents the slow time scale associated with the diffusive process and $\mathbf{x^{(1)}}$ represents the corresponding relatively large spatial scale and the expansion of $f_i(x, t)$ is

$$f_i = f_i^{(0)} + \epsilon f_i^{(1)} + \epsilon^2 f_i^{(2)} + O(\epsilon^3) \tag{17}$$

Substituting (16) in (13) and truncating the terms with an order of magnitude larger than $O(\epsilon^3)$. To recover (9), summation over all states for (13) is given as:

$$\begin{aligned} \sum_i \epsilon^2\Delta t\partial_t^{(2)} f_i + \sum_i \epsilon\Delta t\partial_{x_\alpha^{(1)}} c_{i_\alpha} f_i + \sum_i \frac{1}{2}\Delta t^2\epsilon^2 c_{i_\alpha} c_{i_\beta}\partial_{x_\alpha^{(1)}}\partial_{x_\beta^{(1)}} f_i \\ = \Lambda\big(\sum_i (f_i(x,t) - f_i^{eq}(x,t))\big) + \Delta t\sum_i \Theta_i \end{aligned} \tag{18}$$

The first term on the LHS of (18) corresponds to the unsteady term as:

$$\sum_i \epsilon^2 \Delta t \partial_t^{(2)} f_i = \sum_i \partial_t f_i = \partial_t T \tag{19}$$

The second term on the LHS of (18) is given as:

$$\begin{aligned}
\sum_i \epsilon \Delta t \partial_{x_\alpha^{(1)}} c_{i_\alpha} f_i &= \sum_i \epsilon \Delta t \partial_{x_\alpha^{(1)}} c_{i_\alpha} \left[f_i^0 + \epsilon f_i^1 + O(\epsilon^2) \right] \\
&= \epsilon \Delta t \partial_{x_\alpha^{(1)}} \sum_i c_{i_\alpha} f_i^{(0)} + \epsilon^2 \Delta t \partial_{x_\alpha^{(1)}} \sum_i c_{i_\alpha} f_i^{(1)} + O(\epsilon^3) \\
&= \epsilon \Delta t \partial_{x_\alpha^{(1)}} \sum_i c_{i_\alpha} \left(\frac{1}{\Lambda} \epsilon \partial_{x_\beta^{(1)}} c_{i_\beta} f_i^0 \right) = \epsilon^2 \Delta t^2 \frac{1}{\Lambda} \partial_{x_\alpha^{(1)}} \partial_{x_\beta^{(1)}} c_{i_\alpha} c_{i_\beta} f_i^{(0)} \\
&= \frac{1}{\Lambda} c^2 \Delta t^2 \nabla^2 T (D1Q2) \\
&= \frac{1}{3\Lambda} c^2 \Delta t^2 \nabla^2 T (D2Q5)
\end{aligned}$$

The third term on LHS of (18) becomes:

$$\begin{aligned}
&\frac{1}{2} \Delta t^2 \epsilon^2 \sum_i c_{i_\alpha} c_{i_\beta} \partial_{x_\alpha^{(1)}} \partial_{x_\beta^{(1)}} f_i \\
&\qquad = \frac{1}{2} \Delta t^2 \sum_i \epsilon^2 c_{i_\alpha} c_{i_\beta} \partial_{x_\alpha^{(1)}} \partial_{x_\beta^{(1)}} \left[f_i^0 + \epsilon f_i^1 + O(\epsilon^2) \right] \\
&\qquad = \frac{1}{2} \Delta t^2 \epsilon^2 \partial_{x_\alpha^{(1)}} \partial_{x_\beta^{(1)}} \sum_i c_{i_\alpha} c_{i_\beta} f_i^{(0)} + O(\epsilon^3) \\
&\qquad = \frac{\Delta t^2}{2} c^2 \nabla^2 T (D1Q2) \\
&\qquad = \frac{\Delta t^2}{6} c^2 \nabla^2 T (D2Q5)
\end{aligned}$$

The RHS of (18) is:

$$\Lambda \left(\sum_i f_i - \sum_i f_i^{eq} \right) + \sum_i \Theta_i = \Lambda (T - T) + L_a \frac{g}{\rho c_p} = L_a \frac{g}{\rho c_p}$$

Thus, (18) becomes:

$$\frac{\partial T}{\partial t} = -\left(\frac{1}{\Lambda} + \frac{1}{2} \right) \Delta t c^2 \nabla^2 T + L_a \frac{g}{\rho c_p} \tag{20}$$

Comparing (9) and (20)

$$-\left(\frac{1}{\Lambda}+\frac{1}{2}\right)\Delta t c^2 = \frac{\alpha}{1+\tau\frac{\partial}{\partial t}} \tag{21}$$

The Hyperbolic collision operator Λ is given by:

$$\Lambda = -\frac{2\Delta t\left(1+\tau\frac{\partial}{\partial t}\right)}{2\alpha+\Delta t c^2\left(1+\tau\frac{\partial}{\partial t}\right)} \tag{22}$$

Substituting the value of Λ in equation (10)

$$\psi_i = \phi\psi_i^0 - 2(\phi+\varphi)\theta_i + 2\phi\theta_i^0 + \frac{w_i dt}{\rho C_p}(g_i - g_i^0) \tag{23}$$

Here, $\psi_i(x,t) = f_i(x+\Delta x, t+\Delta t) - f_i(x,t)$, $\psi_i^0(x,t) = \psi_i(x,t-\Delta t)$, $\theta_i(x,t) = f_i(x,t) - f_i^{eq}(x,t)$, $\theta_i^0 = \theta_i(x,t-\Delta t)$, $\phi = \frac{\gamma}{2\alpha^*+1+\gamma}$, $\varphi = \frac{1}{2\alpha^*+1+\gamma}$, $\alpha^* = \frac{\alpha}{\Delta t c^2}$, $\gamma = \frac{\tau}{\Delta t}$, $c = \frac{\Delta x}{\Delta t}$ and $g_i^0(x,t) = g_i(x,t-\Delta t)$

The operator Λ is known as the Hyperbolic Collision operator and the LBM using this operator is known as Hyperbolic Lattice Boltzmann Method (HLBM).

3.2 Method

The two phases that make up the HLBM process are collision and streaming. When particles collide, there is a difference between the distribution function's initial and final states. The collision operator in the HLBM describes this rate of change. When particles collide, they stream through links in many directions, referred to as streaming. The adopted LBM model determines the direction of the distribution function. Here, we have chosen the D1Q2 and D2Q5 models.

(a) D1Q2

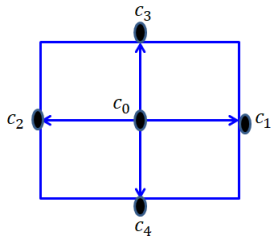

(b) D2Q5

Fig. 1 Lattice arrangements

4 Discrete Boltzmann method

The evolution of the distribution function is given by:

$$\frac{\partial f}{\partial t} + \mathbf{c}.\nabla f + \mathbf{a}.\nabla f = \left(\frac{\partial f}{\partial t}\right)_c \tag{24}$$

Here, f is the particle distribution function, $\mathbf{c}$ the velocity in the desired direction, $\mathbf{a}$ is the acceleration driven on by an external force, and $\left(\frac{\partial f}{\partial t}\right)_c$ indicates the rate at which the distribution function changes as a result of contact. The discretized form of the equation is given by:

$$\frac{\partial f_i}{\partial t} + c_i \frac{\partial f_i}{\partial x} = \frac{1}{\tau}(f_i - f_i^{eq}) + F_i \tag{25}$$

Here, f_i and f_i^{eq} are the particle distribution function and particle equilibrium distribution function respectively in the direction i with velocity c_i, F denotes the external force.

The evolution equation of the discrete distribution function at time $t + dt$ is given by:

$$f_i(x, t + dt) = f_i(x, t) - \frac{1}{\tau}\left(f_i(x, t) - f_i^{eq}(x, t)\right) - c_i \frac{\partial f_i}{\partial x} + F_i \tag{26}$$

Both time and spatial derivatives need to be calculated in this process. Various schemes, including finite difference, the nine-point stencil, etc., can be used depending on the accuracy requirements. In this case, the time and space derivatives are approximated using the forward Euler scheme.

4.1 MRT Discrete Boltzmann Method

Moments rather than population are relaxed by the MRT collision operator. The population is moved from velocity space to moment space, where collisions occur, and then returned to velocity space, where the macroscopic properties are determined. The Discrete Boltzmann Equation (DBE) takes the form,

$$\frac{\partial \mathbf{f}}{\partial t} + \mathbf{c}.\nabla f = -(\mathbf{M^{-1}SM})(\mathbf{f} - \mathbf{f}^{eq}) + \mathbf{g} \tag{27}$$

Here, $\mathbf{f}$ and $\mathbf{f^{eq}}$ denote the discrete distribution function and the equilibrium discrete distribution function respectively. $\mathbf{M}$ is the transformation matrix, $\mathbf{M}^{-1}$ is the inverse of transformation matrix $\mathbf{M}$. The diagonal matrix $\mathbf{S}$ contains elements that describe the rate at which $\mathbf{f}$ approaches $\mathbf{f^{eq}}$. $\mathbf{I}$ is the identity matrix. $\mathbf{g}$ is the source term or phase change term. The DBE form is given by [19]

$$f_i(x, t + dt) = f_i(x, t) - (\mathbf{M^{-1}SM})_{ik}(f_k(x, t) - f_k^{eq}(x, t))dt$$

$$- \mathbf{c_i}.\nabla f dt + dt \left[\mathbf{M^{-1}} \left(\mathbf{I} - \frac{\mathbf{S}}{\mathbf{2}}\right) \mathbf{M}\right]_{ik} g_k \tag{28}$$

4.2 Method

Here, we have used the one-dimensional D1Q7 discrete velocity model as given in [20] . This model has three distribution functions say f_0, f_1, f_2, f_3, f_4, f_5, f_6 moving in opposite direction with seven discrete velocities c_0, c_1, c_2, c_3, c_4, c_5, c_6 having weight functions w_0, w_1, w_2, w_3, w_4, w_5, w_6 respectively.

Fig. 2 Lattice arrangement for 1D D1Q7 model

5 Source Term

The enthalpy method is used to simulate the phase transition problem, in which the interface conditions are satisfied naturally. Since the source term involves the derivative term, the iterative procedure [6] is used. The source term is given by:

$$g = -\frac{\partial(\rho f_l)}{\partial t} \tag{29}$$

Using the forward Euler scheme to approximate the derivate, we obtain that

$$g = -\rho \frac{f_l(x, t + dt) - f_l(x, t)}{dt} \tag{30}$$

The liquid phase fraction f_l is given by

$$f_l = \begin{cases} 0 & H < H_s \\ \frac{H - H_s}{H_l - Hs} & H_s \leq H \leq H_l \\ 1 & H > H_l \end{cases}$$

The enthalpies H_l and H_s, respectively corresponds to the temperatures T_l and T_s, standing for the temperature of the solid and liquid, respectively. The total enthalpy H is given as

$$H = C_p T + L_a f_l \tag{31}$$

6 Results and Discussion

The schematic diagram of the phase change phenomenon is given in figure 3. With a temperature of T_m, the system was initially in the solid state. The temperature at $x = 0$ was abruptly raised to T_0 at time $t = 0$ and kept there for all times t > 0. The discrete liquid/solid interface traveled in the positive x direction as the boundary condition was imposed, and melting started at the surface where $x = 0$ and progressed into the solid.

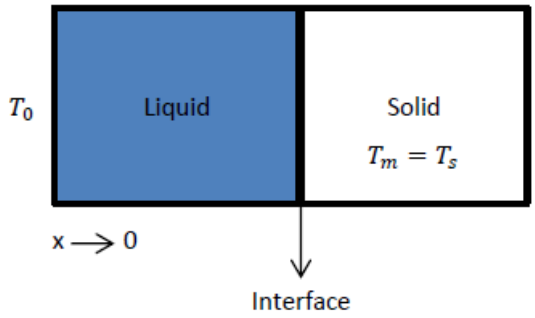

Fig. 3 Schematic diagram of solid-liquid phase change problem

6.1 Implementation

Figure 4 shows the flow chart of the HLBM and DBM processes. The algorithm consists of cyclic processes: the main loop aims to calculate the temperature evolution over time, while the iterative loop embedded inside the main loop is used for calculating the enthalpy and liquid phase fraction. Collision and streaming form the foundation of the HLBM algorithm, and the core of the DBM process involves using any numerical scheme depending on the problem.

6.2 Melting in Half Region (HLBM)

The non-Fourier heat conduction involving the phase change is observed here. It involves the effect of relaxation time τ, which makes it different from the Fourier heat conduction phenomenon. The physical parameters are chosen as τ=0.01, $T_0 = 1$; $T_m = -1$; $\alpha_l = 0.03$; $L_a = 1$. The temperature profile at time $t = 1$ is shown in figure 6. Moreover, it is evident that a change in the heat transfer rate as thermal diffusivity increases. The melting process accelerates considerably and is shown in figure 7.

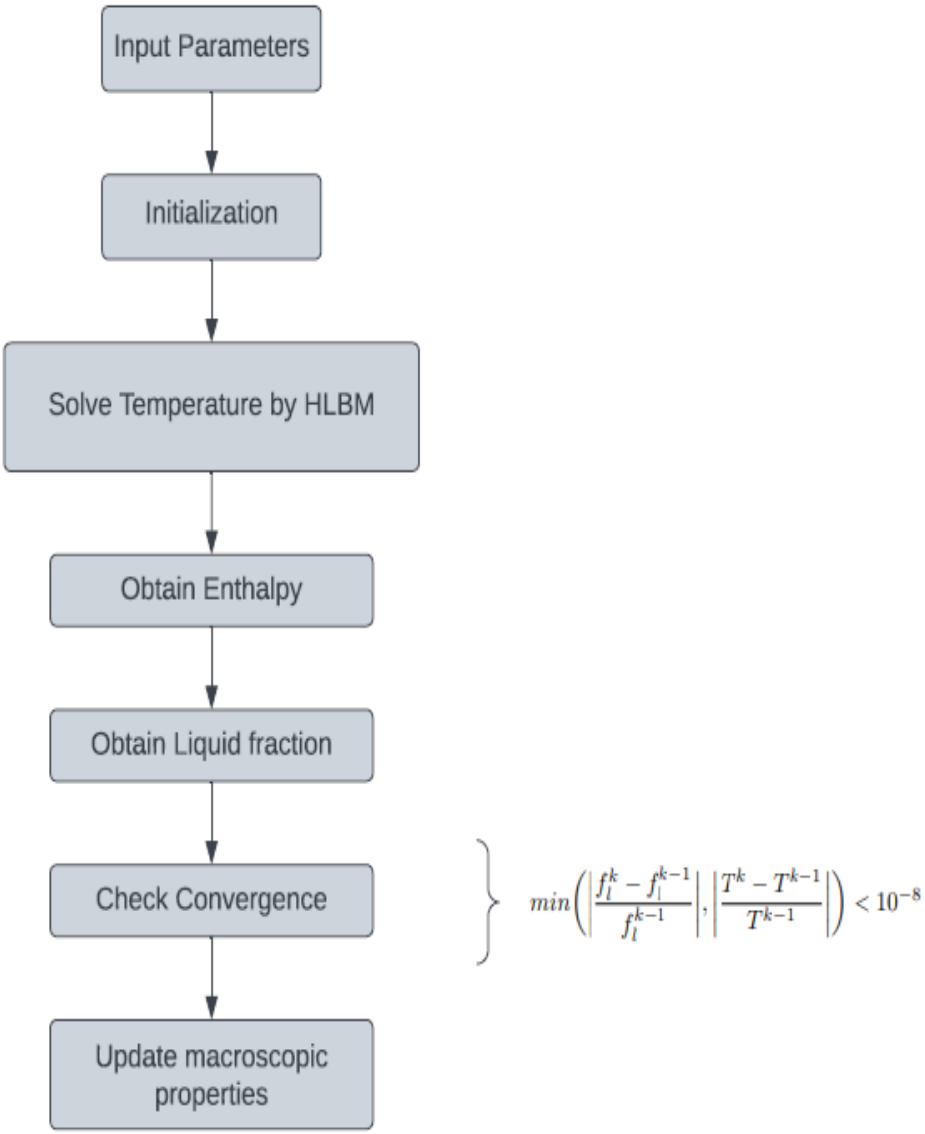

Fig. 4 Flow chart of HLBM

6.3 Melting in Half Region (DBM)

The schematic diagram of the phase change phenomenon is given in figure 3. Here, the system is initially at solid-state and kept at melting temperature T_m. The temperature on the left wall increased slowly until it reached T_0 and kept at that temperature for all time $t > 0$. Since the melting starts at surface $x = 0$, the interface starts to move in a positive direction. The temperature in

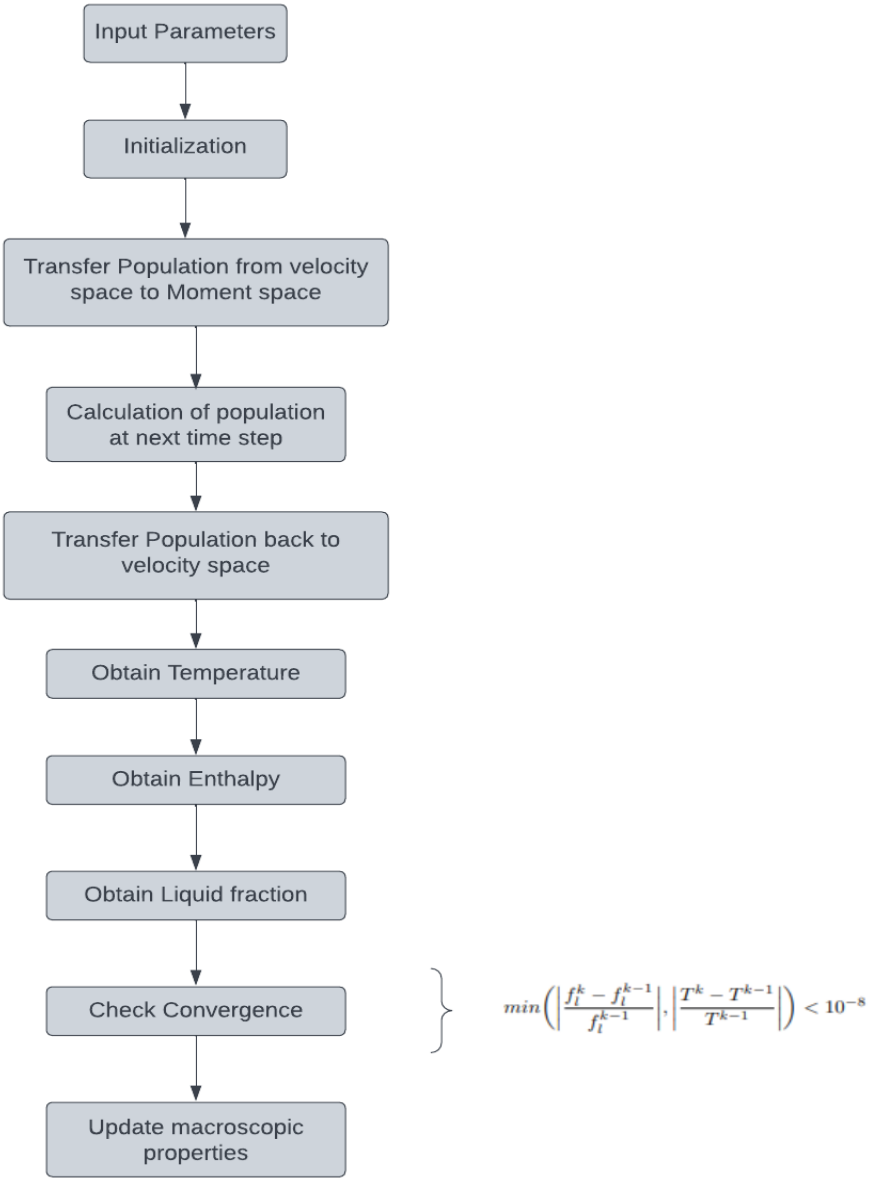

Fig. 5 Flow chart of MRT DBM

the liquid region is unknown. The physical parameters are chosen as $T_m = 0$; $T_0 = 1$; $L_a = 1, c_p = 1$; $\alpha = 0.08$; τ=0.741

The famous BGK approximation uses the single relaxation time, where all the distribution function relaxes with the single time towards the equilibrium

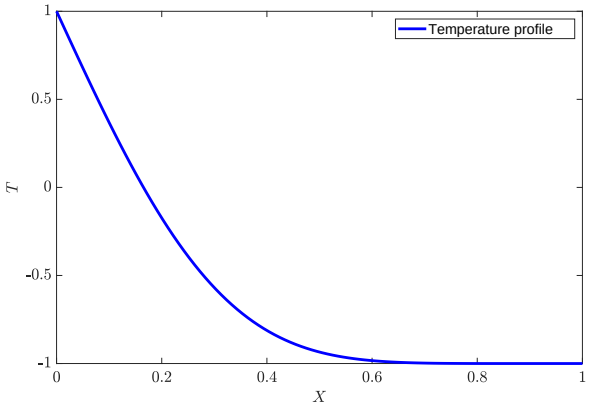

Fig. 6 Temperature distribution using HLBM

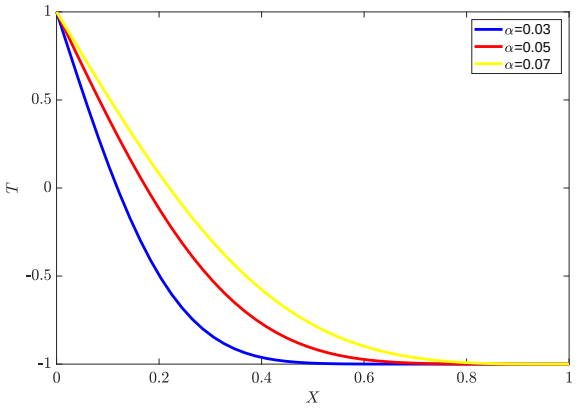

Fig. 7 Temperature distribution using HLBM at different α's

distribution. The temperature distribution in the liquid region using the DBM is shown in figure 8 and a close agreement is found between the analytical solution and DBM solution

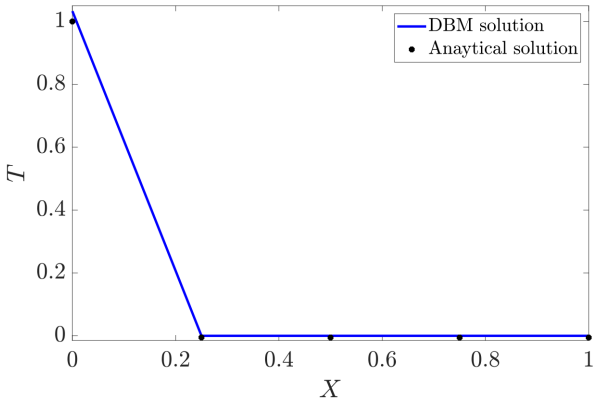

Fig. 8 Temperature distribution using SRT DBM

6.3.1 MRT Discrete Boltzmann method

In D1Q7 lattice structure, the velocity $\mathbf{c_i}$, $\mathbf{M}$ and $\mathbf{S}$ is given by

$$\mathbf{v_i} = \begin{cases} 0 & i=0 \\ c_0 & i=1 \\ -c_0 & i=2 \\ \sqrt{2}c_0 & i=3 \\ -\sqrt{2}c_0 & i=4 \\ 2c_0 & i=5 \\ -2c_0 & i=6 \end{cases}, \mathbf{M} = \begin{pmatrix} 1 & 1 & 1 & 1 & 1 & 1 & 1 \\ 0 & c_0 & -c_0 & \sqrt{2}c_0 & -\sqrt{2}c_0 & 2c_0 & -2c_0 \\ 0 & c_0^2 & c_0^2 & 2c_0^2 & 2c_0^2 & 4c_0^2 & 4c_0^2 \\ 0 & c_0^3 & -c_0^3 & 2\sqrt{2}c_0^3 & -2\sqrt{2}c_0^3 & 8c_0^3 & -8c_0^3 \\ 0 & c_0^4 & c_0^4 & 4c_0^4 & 4c_0^4 & 16c_0^4 & 16c_0^4 \\ 0 & c_0^5 & -c_0^5 & 4\sqrt{2}c_0^5 & -4\sqrt{2}c_0^5 & 32c_0^5 & -32c_0^5 \\ 0 & c_0^6 & c_0^6 & 8c_0^6 & 8c_0^6 & 124c_0^6 & 124c_0^6 \end{pmatrix}$$

$$\mathbf{S} = \begin{pmatrix} S_0 & 0 & 0 & 0 & 0 & 0 & 0 \\ 0 & S_1 & 0 & 0 & 0 & 0 & 0 \\ 0 & 0 & S_2 & 0 & 0 & 0 & 0 \\ 0 & 0 & 0 & S_3 & 0 & 0 & 0 \\ 0 & 0 & 0 & 0 & s_4 & 0 & 0 \\ 0 & 0 & 0 & 0 & 0 & S_5 & 0 \\ 0 & 0 & 0 & 0 & 0 & 0 & S_6 \end{pmatrix}$$

The relaxation matrix $\mathbf{S}$ relaxes the moment, which represents the core of the MRT collision operator. The values of S_i are chosen in such a way that the stability of the problem is maintained as given by [21]. The temperature distribution using MRT DBM is shown in figure (13) and a close agreement is found with the analytical solution.

6.4 Solidification in Half Region

The process of solidification is the change from a liquid to a solid state. Here, a square cavity is used to solidify the liquid. The system is initially in a liquid state at time $t = 0$ i.e. it is at the phase change temperature T_m for $x > 0$, $y > 0$. The temperature at x=0 and y=0 gradually decreased until it reached

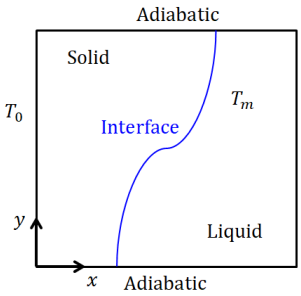

Fig. 9 Schematic diagram of solid-liquid phase change problem.

the temperature T_0 and remained there for all $t > 0$. The interface's left side appears to be solid when the temperature is decreased, while the right side is in a liquid state. Because the temperature in one phase is already known and the temperature in the other part is the sole of interest, this problem is also referred to as a one-region problem. The schematic diagram of the process is given in figure (9).

6.4.1 Melting in Half Region(HLBM)

When τ =0; then the Fourier heat conduction phenomenon is carried out. The physical parameters are chosen as $T_0 = 1$; $T_m = -1$; $\alpha_l = 0.03$; $L_a = 1$. The 1D phase change phenomenon is carried out using the proposed model and a close agreement between HLBM solution and analytical solution as mentioned in [22] is observed in figure (10).

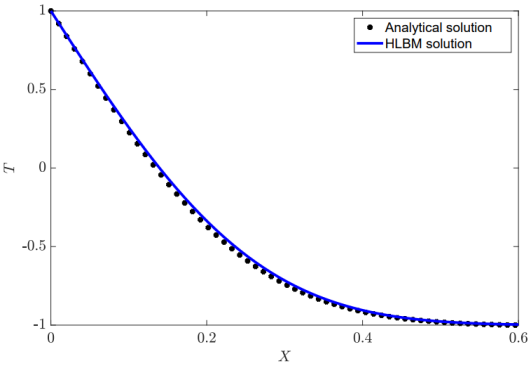

Fig. 10 Comparison between Analytical and HLBM solution

6.4.2 Solidification in Half Region(HLBM)

The 2D non-Fourier heat conduction phenomena, which considers the contribution of relaxation time into effect, will be witnessed in this case. The physical parameters are chosen as τ=0.1, T_0=-1, T_m=0, α_l = 0.10, and St = $C(T_m - T_0)/L_a$, L_a=1. It was also assumed that material properties are constant. The temperature profile at time t=1 has been shown in figure (11) and (12)

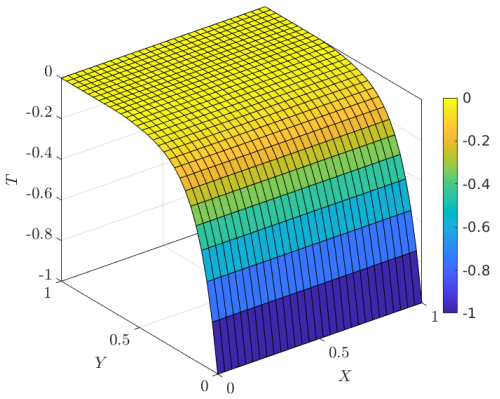

Fig. 11 Temperature distribution of 2D CV heat conduction problem with phase change using HLBM

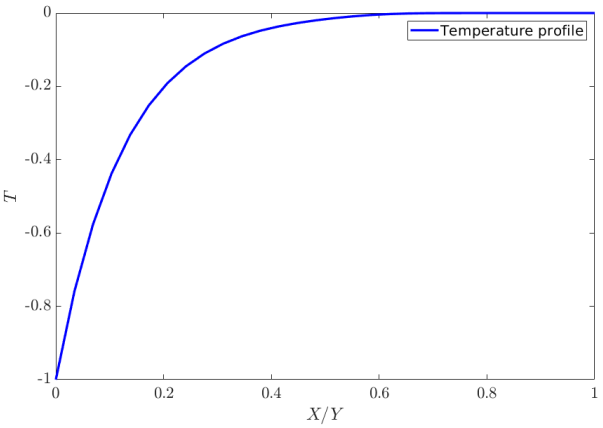

Fig. 12 Temperature distribution using HLBM

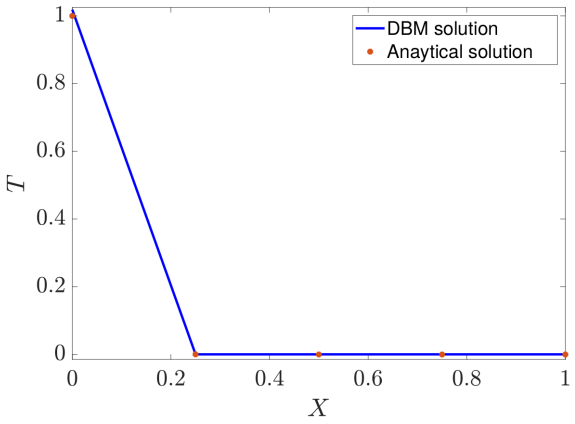

Fig. 13 Temperature distribution using MRT DBM

6.4.3 Effect of Thermal Diffusivity (α)

The rate of heat transfer through a medium is governed by thermal diffusivity. We have obtained the temperature profile at various α and observed that as α is increased, the solidification process increases. The temperature distribution at various α is observed in figure (15) and (14).

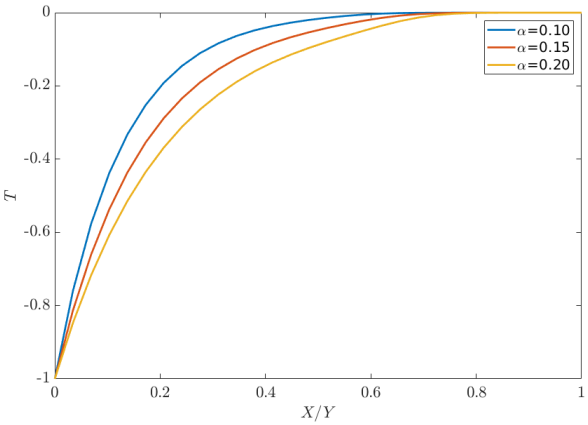

Fig. 14 Temperature distribution using HLBM at various $\alpha_s^{'}$

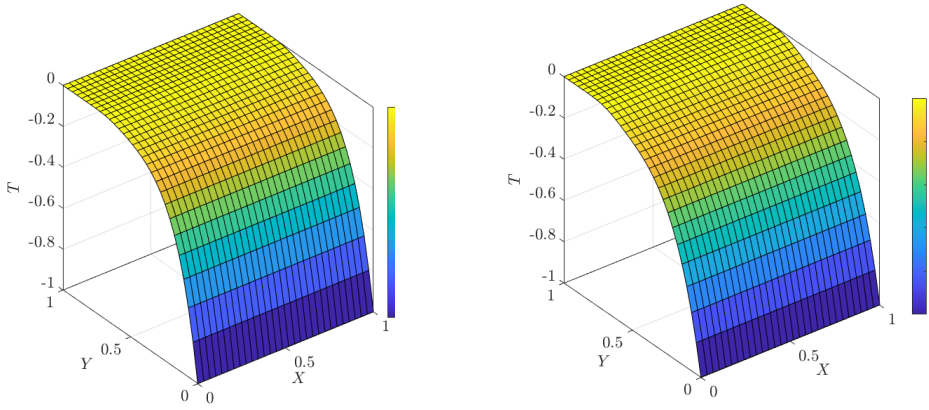

(a) $\alpha = 0.15$ (b) $\alpha = 0.20$

Fig. 15 Temperature distribution using HLBM

6.4.4 Solidification in Half Region(DBM)

The [23] discussed the higher order DBM. The discretized form of the equation is given by:

$$\frac{\partial f_i}{\partial t} + c_{i_x}\frac{\partial f_i}{\partial x} + c_{i_y}\frac{\partial f_i}{\partial y} = -\frac{1}{\tau}(f_i - f_i^{eq}) + F_i \tag{32}$$

$$\frac{\partial f_i}{\partial t} = -\frac{1}{\tau}(f_i - f_i^{eq}) - \left(c_{i_x}\frac{\partial f_i}{\partial x} + c_{i_y}\frac{\partial f_i}{\partial y}\right) + F_i \tag{33}$$

Here, c_{ix} and c_{iy} are the velocities in the x and y direction respectively. The physical parameters are chosen as $\tau = 0.1$, $T_0 = -1$, $T_m = 0$, $\alpha_l = 0.10$, and St $= C(T_m - T_0)/L_a$, $L_a = 4$. It was also assumed that material properties are constant. The temperature profile at time $t = 1$ has been shown in figure (16)

6.4.5 Solidification in Half Region(MRT DBM)

The D2Q5 has been used to carry out the 2D solidification process. The physical parameters chosen are $\tau = 0.741$, $T_0 = -1$, $T_m = 0$, $\alpha_l = 0.04$, and St $= C(T_m - T_0)/L_a$, $L_a = 4$. In D2Q5 lattice structure, the velocity $\mathbf{c_i}$, $\mathbf{M}$ is given by

$$\mathbf{v_i} = \begin{cases} (0,0) & i = 0 \\ (0,c_0) & i = 1 \\ (-c_0,0) & i = 2 \\ (0,c_0) & i = 3 \\ (0,-c_0) & i = 4 \end{cases} \quad \mathbf{M} = \begin{pmatrix} 1 & 1 & 1 & 1 & 1 \\ 0 & c_0 & 0 & -c_0 & 0 \\ 0 & 0 & c_0 & 0 & -c_0 \\ 0 & c_0 & c_0 & c_0 & c_0 \\ 0 & c_0 & -c_0 & c_0 & -c_0 \end{pmatrix}$$

The temperature distribution is given in figure (17)

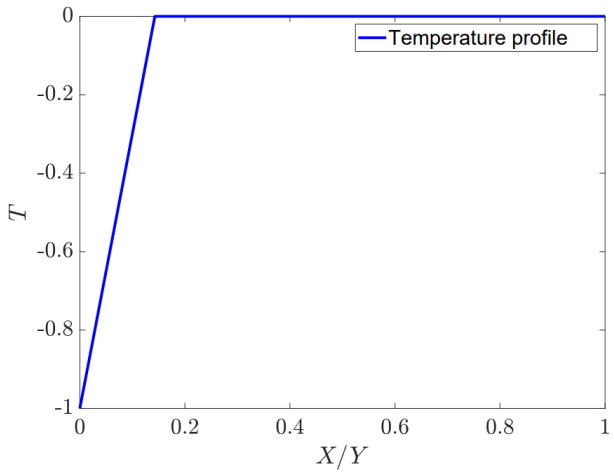

Fig. 16 Temperature distribution using SRT DBM.

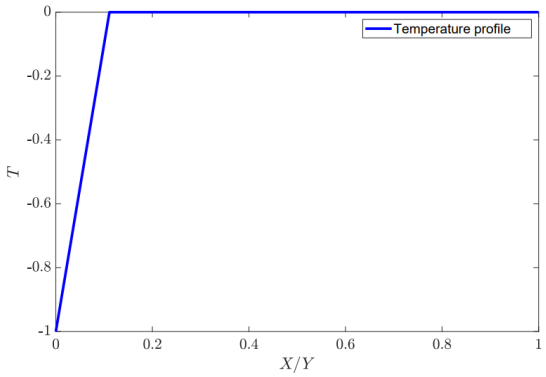

Fig. 17 Temperature distribution using MRT DBM.

7 Conclusion

The phase change phenomena of the solid-liquid problems governed by the heat conduction using the HLBM, DBM, and MRT DBM coupled with the enthalpy method are compared. While using the HLBM both the Fourier and non-Fourier phenomena are used for comparison. The impact of thermal diffusivity (α) on the HLBM temperature distribution is also compared. The melting and solidification processes increase as the α increases. Since the HLBM uses the Hyperbolic collision operator which makes it different from the LBM which uses BGK operator and other methods, it is one of the new methods devised to solve hyperbolic equations. The non-Fourier phenomena for the DBM and MRT DBM are yet to be explored.

8 Statement and Declaration

- Competing Interests: The authors declare no conflict of interest.

References

[1] John, D.: The Theory of Laser Materials Processing: Heat and Mass Transfer in Modern Technology, (2009). https://doi.org/10.1007/978-1-4020-9340-1

[2] Yadroitsev, I., Smurov, I.: Selective laser melting technology: From the single laser melted track stability to 3d parts of complex shape. Physics Procedia **5**, 551–560 (2010). Laser Assisted Net Shape Engineering 6, Proceedings of the LANE 2010, Part 2

[3] Voller, V.R., Swaminathan, C., Thomas, B.G.: Fixed grid techniques for phase change problems: a review. International journal for numerical methods in engineering **30**(4), 875–898 (1990)

[4] Shamsundar, N., Sparrow, E.: Analysis of multidimensional conduction phase change via the enthalpy model. Journal of Heat Transfer **97**(3), 333–340 (1975). https://doi.org/10.1115/1.3450375

[5] Bonacina, C., Comini, G., Fasano, A., Primicerio, M..: Numerical solution of phase-change problems. International Journal of Heat and Mass Transfer **16**(10), 1825–1832 (1973)

[6] Wen-Shu Jiaung, C.-P.K. Jeng-Rong Ho: Lattice boltzmann method for the heat conduction problem with phase change. Numerical Heat Transfer, Part B: Fundamentals **39**(2), 167–187 (2001). https://doi.org/10.1080/10407790150503495

[7] Huang, R., Wu, H., Cheng, P.: A new lattice boltzmann model for solid–liquid phase change. International Journal of Heat and Mass Transfer **59**, 295–301 (2013). https://doi.org/10.1016/j.ijheatmasstransfer.2012.12.027

[8] Ibrahem, A.: Lattice boltzmann technique for heat transport phenomena coupled with melting process. Heat and Mass Transfer **52** (2017). https://doi.org/10.1007/s00231-016-1811-8

[9] Chatterjee, D.: Lattice Boltzmann Modeling for Melting/Solidification Processes, (2011). https://doi.org/10.5772/28236

[10] Gan, Y., Xu, A., Zhang, G., Succi, S.: Discrete boltzmann modeling of multiphase flows: hydrodynamic and thermodynamic non-equilibrium effects. Soft Matter **11**, 5336–5345 (2015). https://doi.org/10.1039/

C5SM01125F

[11] Zhang, Y., Xu, A., Qiu, J., Wei, H., Wei, Z.-H.: Kinetic modeling of multiphase flow based on simplified enskog equation (2020)

[12] Lin, C., Luo, K.H.: Mrt discrete boltzmann method for compressible exothermic reactive flows. Computers & Fluids **166**, 176–183 (2018). https://doi.org/10.1016/j.compfluid.2018.02.012

[13] Kruger, T., Kusumaatmaja, H., Kuzmin, A., Shardt, O., Silva, G., Viggen, E.M.: The Lattice Boltzmann Method - Principles and Practice. Springer, London (2017)

[14] Mohamad, A.A.: The Boltzmann Equation, pp. 25–39. Springer, London (2019). https://doi.org/10.1007/978-1-4471-7423-3_2

[15] Cattaneo, C.: Sulla conduzione del calore. Atti Sem. Mat. Fis. Univ. Modena **3**, 83–101 (1948)

[16] Vernotte, P.: Sur quelques complications possibles dans les phenomenes de conduction de la chaleur. Compte Rendus **252**, 2190–2191 (1961)

[17] Liu, Y., Li, L., Lou, Q.: A hyperbolic lattice boltzmann method for simulating non-fourier heat conduction. International Journal of Heat and Mass Transfer **131**, 772–780 (2019)

[18] Liu, Y., Li, L.: Lattice boltzmann simulation of non-fourier heat conduction with phase change. Numerical Heat Transfer, Part A: Applications **76**(1), 19–31 (2019). https://doi.org/10.1080/10407782.2019.1612155

[19] Chai, Z., Shi, B., Guo, Z.: A multiple-relaxation-time lattice Boltzmann model for general nonlinear anisotropic convection-diffusion equations. J. Sci. Comput. **69**(1), 355–390 (2016). https://doi.org/10.1007/s10915-016-0198-5

[20] Zhang, Y.-D., Xu, A.-G., Zhang, G.-C., Chen, Z.-H.: A one-dimensional discrete boltzmann model for detonation and an abnormal detonation phenomenon. Communications in Theoretical Physics **71**(1), 117 (2019)

[21] Lin, Y., Hong, N., Shi, B., Chai, Z.: Multiple-relaxation-time lattice Boltzmann model-based four-level finite-difference scheme for one-dimensional diffusion equations. Phys. Rev. E **104**, 015312 (2021). https://doi.org/10.1103/PhysRevE.104.015312

[22] Ozisik, M.N.: Heat Conduction (2nd Ed.). Wiley, New York (1993)

[23] Watari, M., Tsutahara, M.: Supersonic flow simulations by a three-dimensional multispeed thermal model of the finite difference lattice

boltzmann method. Physica A: Statistical Mechanics and its Applications **364**, 129–144 (2006). https://doi.org/10.1016/j.physa.2005.06.103